INTERNATIONAL JOURNAL FOR NUMERICAL METHODS IN FLUIDS, VOL. 11, 835–847 (1990)

GODUNOV–MIXED METHODS FOR IMMISCIBLE DISPLACEMENT

CLINT N. DAWSON

Department of Mathematics, University of Chicago, Chicago, IL 60637, U.S.A.

SUMMARY

The immiscible displacement problem in reservoir engineering can be formulated as a system of partial differential equations which includes an elliptic pressure–velocity equation and a degenerate parabolic saturation equation. We apply a sequential numerical scheme to this problem where time splitting is used to solve the saturation equation. In this procedure one approximates advection by a higher-order Godunov method and diffusion by a mixed finite element method. Numerical results for this scheme applied to gas–oil centrifuge experiments are given.

KEY WORDS Higher-order Godunov method Mixed finite element method Immiscible displacement

1. INTRODUCTION

Immiscible displacement of one incompressible fluid by another can be described by a system of partial differential equations of the form

$$-\lambda_T(\mathbf{x}, s)\nabla p + \lambda_1(\mathbf{x}, s)\gamma_1 + \lambda_2(\mathbf{x}, s)\gamma_2 = \mathbf{u}, \tag{1}$$

$$\nabla \cdot \mathbf{u} = 0, \tag{2}$$

$$\phi(\mathbf{x})s_t + \nabla \cdot (\mathbf{A}(\mathbf{x}, s, \mathbf{u}) - \bar{\lambda}(\mathbf{x}, s)\nabla p_c(\mathbf{x}, s)) = 0, \quad \mathbf{x} \in \Omega, \quad 0 < t \leqslant T, \tag{3}$$

with appropriate boundary conditions on p and s and initial conditions on s. We assume $\Omega \in \mathbb{R}^2$. In these equations the unknowns are $\mathbf{u} = (u, v)$, which is the total velocity, obtained by summing the individual fluid velocities; p, which is the 'global' pressure, which involves the fluid pressures and capillary pressure; and s, which is the saturation of the fluid of interest (e.g. oil, gas or water). In (1), $\lambda_T = \lambda_1 + \lambda_2$, with λ_i the mobility of fluid i, and $\lambda_i = K(\mathbf{x})k_{ri}(s)/\mu_i$, where K is the absolute permeability of the porous media, k_{ri} is the relative permeability of fluid i and μ_i is the viscosity of fluid i. Also $\gamma_i = \rho_i g \nabla z$, where ρ_i is the density of fluid i and $g\nabla z$ is the gravitational force. In (3), ϕ is the porosity, p_c is the capillary pressure and $\mathbf{A} \equiv (F, G) = f(s)\mathbf{u} - (\gamma_2 - \gamma_1)\bar{\lambda}$, with $f(s) = \lambda_1/(\lambda_1 + \lambda_2)$ and $\bar{\lambda} = \lambda_2 f$. We are assuming $s \equiv s_1$ and $s_1 + s_2 = 1 - s_{cw}$, where s_{cw} is the connate water saturation. We are also assuming that no source or sink terms (wells) are present. When wells are present, these are modelled as Dirac delta functions. For more details on these equations, see References 1 and 2.

The system (1)–(3) does not lend itself to solution by analytic techniques, hence numerical approximation is necessary. There are several numerical difficulties which must be considered in these problems. First, when capillary pressure effects are ignored ($p_c \equiv 0$), (3) reduces to a first-order hyperbolic equation, and for certain initial and boundary conditions, shocks can develop in

0271–2091/90/140835–13$06.50 *Received November 1989*

the saturation solution. Even in the presence of capillary pressure, the saturation solution often develops sharp fronts. These must be approximated without extreme oscillations and numerical diffusion. As seen in (3), the inclusion of capillary pressure gives rise to a second-order non-linear term which, for stability purposes, is best handled implicitly. Thus a non-linear system of equations must be solved at each time step, which can add considerably to the cost of the calculation. Another numerical difficulty is sensitivity to grid orientation, or the 'grid orientation effect'. This is an undesirable trait exhibited by many schemes, whereby radically different results are obtained depending on the orientation of the grid with respect to the direction of flow. This effect was first observed in the simulation of immiscible displacement by Todd *et al.*[3] and a substantial literature now exists on the subject; see Reference 4 for further references.

The numerical technique we use for solving (1)–(3) was developed with the above difficulties in mind. The method uses a sequential approach, which is outlined as follows. Let $0 \leqslant \bar{t} < t^* \leqslant T$. First, given $S(\mathbf{x}, \bar{t}) \approx s(\mathbf{x}, \bar{t})$, a nine-point block-centred finite difference scheme is applied to (1), (2) to approximate total velocity and pressure, giving $(U, V) \equiv \mathbf{U} \approx \mathbf{u}(\mathbf{x}, \bar{t})$. We then solve for saturation by time splitting; that is, (3) is split into an advection equation and a diffusion equation. Thus we solve numerically

$$\phi(\mathbf{x})\bar{s}_t + F(\mathbf{x}, \bar{s}, U)_x + G(\mathbf{x}, \bar{s}, V)_y = 0, \quad \bar{t} < t \leqslant t^*, \tag{4}$$

$$\bar{s}(\mathbf{x}, \bar{t}) = S(\mathbf{x}, \bar{t}),$$

obtaining $S(\mathbf{x}, t^*) \approx \bar{s}(\mathbf{x}, t^*)$. Then we solve numerically

$$\phi(\mathbf{x})s_t^* - \nabla \cdot (\bar{\lambda}(\mathbf{x}, s^*)\nabla p_c(\mathbf{x}, s^*)) = 0, \quad \bar{t} < t \leqslant t^*, \tag{5}$$

$$s^*(\mathbf{x}, \bar{t}) = \bar{S}(\mathbf{x}, t^*).$$

The result of these steps is an approximation $S(\mathbf{x}, t^*)$ to $s(\mathbf{x}, t^*)$. We then return to (1), (2) and update pressure and velocity.

An explicit, unsplit, higher-order Godunov scheme is used to solve (4). A complete description of this scheme is given in Reference 5. The main advantage of using a higher-order Godunov method on (4) is that sharp fronts can be approximated accurately with no loss of stability, and on coarser grids than many standard procedures can use. The unsplit nature of the scheme reduces sensitivity to grid orientation. Furthermore, by handling advection explicitly, we are left with a symmetric system of equations in the diffusion step. The major disadvantage of using an explicit procedure is that one must enforce a CFL time step constraint in the advection step. Thus, if diffusion and advection are approximated on the same time scale, this constraint could prove costly. However, we can avoid this difficulty by time splitting. Thus we can use different sized time steps to approximate (4) and (5); for more details on this idea, see Reference 6 and 7. In the solution of (5) we use a variant[8] of the standard lowest-order mixed finite element method.[9] This combination of a higher-order Godunov procedure and a mixed method (hence the name Godunov–mixed method) has been tested extensively and successfully for various one-[6] and two-dimensional[5] flow problems, and analysis, including error estimates, can be found in Reference 7. The numerical results in References 5 and 6 were from standard test problems in reservoir engineering, and they show that the scheme approximates sharp fronts accurately and is relatively insensitive to grid orientation. In this paper we will use the method to study a realistic problem in reservoir engineering arising from laboratory experiments.

The rest of this paper is organized as follows. In the next section we discuss the two-dimensional numerical method outlined above for solving (1)–(3). In Section 3 we present

numerical results from the application of this algorithm to the simulation of centrifuge experiments. Here we compare our solution with one obtained from a laboratory experiment, and study the effects on the solution of variations in the core sample characteristics.

2. NUMERICAL METHOD

Before describing our algorithm we give some notation. Assume $\Omega=[0, L_x]\times[0, L_y]$. Let N_x, N_y be positive integers and set $\Delta x=L_x/N_x$, $\Delta y=L_y/N_y$. Let $x_{i+1/2}=i\Delta x$, $i=0, \ldots, N_x$, with a similar definition for $y_{j+1/2}$, and partition Ω into grid blocks $B_{ij}=[x_{i-1/2}, x_{i+1/2}]\times[y_{j-1/2}, y_{j+1/2}]$. Let (x_i, y_j) be the midpoint of B_{ij}. Also, for $\Delta t>0$ and $N^*\Delta t=T$, let $t^n=n\Delta t$, $n=0, \ldots, N^*$. Finally, for $g=g(\mathbf{x}, t)$, denote $g(x_i, y_j, t^n)$ by g_{ij}^n.

In (4), (5) let $\tilde{t}=t^n$ and $t^*=t^{n+1}$. Given $S(\mathbf{x}, t^n)\approx S(\mathbf{x}, t^n)$, we apply a block-centred nine-point difference operator to the solution of (1); (2). This method is designed to suppress grid orientation effects and is described in Reference 4. By a choice of a parameter it reduces to standard five-point finite differences. The net result of this step is a function $\mathbf{U}^n=(U^n, V^n)$ which approximates the normal component of $\mathbf{u}^n$ at the grid block boundaries. Thus we obtain $U_{i+1/2, j}^n\approx u_{i+1/2, j}^n$ and $V_{i, j+1/2}^n\approx v_{i, j+1/2}^n$.

Once the velocity is updated, time splitting is used to obtain S^{n+1}. Let Δt_A denote the advection time step and assume

$$\Delta t_A=(t^{n+1}-t^n)/K^n \tag{6}$$

for an integer $K^n\geqslant 1$. Let Δt_D denote the diffusion time step, i.e.

$$\Delta t_D=t^{n+1}-t^n. \tag{7}$$

The first step in our time-splitting approach is to apply the higher-order Godunov method developed in Reference 5 to (4). This scheme consists of three steps. First, given midpoint values S_{ij}^n, $i=1, \ldots, N_x$, $j=1, \ldots, N_y$, we construct a piecewise (possibly) discontinuous bilinear function by calculating 'limited' x, y and xy slopes in each grid block. Initially, S_{ij}^0 may be determined by interpolation or projection of the initial condition into the space of piecewise constants. Next we integrate (4) over the space–time domains $B_{ij}\times[t^n, t^n+\Delta t_A]$, deriving expressions for the midpoint values at the next advection time level. Finally, approximations to the fluxes F and G on the lateral boundaries of these domains are calculated, and the midpoint values in the bilinear approximation are updated. If $K^n=1$ in (6), then this completes the advection step; otherwise, we repeat these three steps K^n times until the time interval $[t^n, t^{n+1}]$ is exhausted. In the discussion that follows we assume for ease of notation that $K^n\equiv 1$.

The bilinear approximation S^n can be written as

$$S^n|_{B_{ij}}=S_{ij}^n+(x-x_i)\delta_x S_{ij}^n+(y-y_j)\delta_y S_{ij}^n+(x-x_i)(y-y_j)\delta_{xy}S_{ij}^n. \tag{8}$$

Note that S_{ij}^n represents the integral average (i.e. cell average) of S^n over B_{ij}, as well as the value at the midpoint of B_{ij}. The slopes $\delta_x S_{ij}^n$, $\delta_y S_{ij}^n$ and $\delta_{xy}S_{ij}^n$ are computed by a multistep slope-limiting procedure. We first interpolate the cell averages surrounding B_{ij} by a bicubic polynomial to obtain corner values which are accurate approximations to $s_{i\pm 1/2, j\pm 1/2}^n$. These corner values are then modified so that they satisfy two conditions. First, each corner value must fall between the maximum and the minimum of the cell averages surrounding the corner, and secondly, the average of the corner values in any cell must equal the cell average. Once these conditions are satisfied, the slopes are calculated by differencing. This procedure is heuristic, but numerical testing[5] indicates that it is close to the following constrained minimization problem. Consider one grid block, B_{ij}, and let S_u^n denote the 'unlimited' bilinear function on B_{ij} obtained from the

unmodified corner values. Note that, formally, S_u^n is a second-order accurate approximation to s^n. Then we seek the bilinear function S_l^n which satisfies

$$\text{minimize} \int_{B_{ij}} |S_u^n - S_l^n|^2 \, dx dy,$$

subject to the constraints

$$\alpha_{i\pm 1/2,\, j\pm 1/2}^n \leqslant (S_l)_{i\pm 1/2,\, j\pm 1/2}^n \leqslant \beta_{i\pm 1/2,\, j\pm 1/2}^n,$$
$$(S_l)_{ij}^n = (S_u)_{ij}^n,$$

where

$$\alpha_{i+1/2,\, j+1/2}^n = \min\{S_{ij}^n, S_{i+1,\, j}^n, S_{i+1,\, j+1}^n, S_{i,\, j+1}^n\},$$
$$\beta_{i+1/2,\, j+1/2}^n = \max\{S_{ij}^n, S_{i+1,\, j}^n, S_{i+1,\, j+1}^n, S_{i,\, j+1}^n\}.$$

The next step in the scheme is to integrate (4) over $B_{ij} \times [t^n, t^{n+1}]$, giving the equation

$$\bar{S}_{ij}^{n+1} = S_{ij}^n - \frac{\Delta t}{\phi_{ij} \Delta x} [F_{i+1/2,\, j}^{n+1/2} - F_{i-1/2,\, j}^{n+1/2}] - \frac{\Delta t}{\phi_{ij} \Delta y} [G_{i,\, j+1/2}^{n+1/2} - G_{i,\, j-1/2}^{n+1/2}], \tag{9}$$

where

$$F_{i+1/2,\, j}^{n+1/2} \approx \frac{1}{\Delta t \Delta y} \int_{t^n}^{t^{n+1}} \int_{y_{j-1/2}}^{y_{j+1/2}} F(x_{i+1/2}, y, \bar{s}, U_{i+1/2,\, j}^n) dy dt, \tag{10}$$

$$G_{i,\, j+1/2}^{n+1/2} \approx \frac{1}{\Delta t \Delta x} \int_{t^n}^{t^{n+1}} \int_{x_{i-1/2}}^{x_{i+1/2}} G(x, y_{j+1/2}, \bar{s}, V_{i,\, j+1/2}^n) dx dt, \tag{11}$$

$$\bar{S}_{ij}^{n+1} \approx \frac{1}{\Delta x \Delta y} \int_{B_{ij}} \bar{s}(x, y, t^{n+1}) dx dy. \tag{12}$$

Here we have assumed ϕ is constant over B_{ij}. If this is not the case, then (9) is obtained by applying the midpoint rule to the integral of $\phi \bar{s}_t$ over B_{ij}.

The numerical flux $F_{i+1/2,\, j}^{n+1/2}$ (similarly $G_{i,\, j+1/2}^{n+1/2}$) is determined by the following multistep procedure. First, left and right states, $S_{i+1/2,\, j,\, L}^{n+1/2}$ and $S_{i+1/2,\, j,\, R}^{n+1/2}$, approximating the average saturation over the region $LR \equiv [y_{j-1/2}, y_{j+1/2}] \times [t^n, t^{n+1}]$ as viewed from the left and the right of the interface, are calculated. These values are obtained by linearizing (4) in the normal flux component and integrating over the characteristic domain of dependence of LR as determined from this linearized equation. In short, characteristic tracing is used to predict the average value of s on LR. Once the left and right states are found, the flux is determined by solving a Riemann problem; that is, we solve a problem of the form

$$\tilde{s}_t + F(x_{i+1/2}, y_j, \tilde{s}, U_{i+1/2,\, j}^n)_x = 0, \tag{13}$$

$$\tilde{s}(x, 0) = \begin{cases} S_{i+1/2,\, j,\, L}^{n+1/2}, & x < 0, \\ S_{i+1/2,\, j,\, R}^{n+1/2}, & x > 0, \end{cases} \tag{14}$$

and evaluate the flux at the value of $\tilde{s}$ which moves with speed $x/t = 0$. In general, the Riemann problem cannot be solved exactly and its solution must be approximated. In our method we have approximated the Riemann problem solution by use of the 'Godunov flux' calculation, which reduces (13), (14) to an optimization problem. Again, for more details on these and other aspects of the flux calculation, see Reference 5 and the references therein.

The explicit nature of the higher-order Godunov scheme, and the use of discontinuous approximating spaces and Riemann problems, require the advection time step to satisfy a CFL constraint; i.e.

$$\max\left(\frac{\Delta t_A}{\Delta x}\sup|F_s|, \frac{\Delta t_A}{\Delta y}\sup|G_s|\right)\leqslant 1.$$

In solving (5), we take as our initial condition the piecewise constant function $\bar{S}^{n+1}$ satisfying $\bar{S}^{n+1}|_{B_{ij}}=\bar{S}_{ij}^{n+1}$. Thus we diffuse our advection solution before projecting into the space of piecewise bilinears. The method we employ is a variant of the lowest-order mixed finite element method, described below.

Let δ_x denote the partition

$$0=x_{1/2}<\ldots<x_{N_x+1/2}=L_x,$$

and define δ_y similarly. Let $I_i=(x_{i-1/2}, x_{i+1/2})$, let

$$\mathscr{M}^r_{-1}(\delta_x)=\{v(x) \text{ such that } v|_{I_i}\in\mathscr{P}^r\},$$

where $\mathscr{P}^r$ denotes the set of polynomials of degree $\leqslant r$, and let

$$\mathscr{M}^r_0(\delta_x)=\mathscr{C}^0(0, L_x)\cap\mathscr{M}^r_{-1}(\delta_x).$$

Define $\mathscr{M}^r_{-1}(\delta_y)$ and $\mathscr{M}^r_0(\delta_y)$ similarly and let $\mathscr{V}$ denote the space of vector-valued functions whose first component is in the tensor-product space $\mathscr{M}^1_0(\delta_x)\otimes\mathscr{M}^0_{-1}(\delta_y)$ and whose second component is in the space $\mathscr{M}^0_{-1}(\delta_x)\otimes\mathscr{M}^1_0(\delta_y)$. Let $\mathscr{W}=\mathscr{M}^0_{-1}(\delta_x)\otimes\mathscr{M}^0_{-1}(\delta_y)$.

Recall that, in (5),

$$\bar{\lambda}(\mathbf{x}, s)=\frac{\lambda_1(\mathbf{x}, s)\lambda_2(\mathbf{x}, s)}{\lambda_T(\mathbf{x}, s)}\equiv K(\mathbf{x})h(s).$$

Let

$$\mathbf{z}^{n+1}=-K(\mathbf{x})\nabla p_c(\mathbf{x}, s^{n+1}). \tag{15}$$

Multiplying both sides of (15) by $K^{-1}(\mathbf{x})\mathbf{v}$, where $\mathbf{v}\in\mathscr{V}$, integrating over Ω and integrating by parts, we obtain

$$\int_\Omega K^{-1}(\mathbf{x})\mathbf{Z}^{n+1}\cdot\mathbf{v}\,dx dy-\int_\Omega p_c(\mathbf{x}, S^{n+1})\nabla\cdot\mathbf{v}\,dx dy=-\int_{\partial\Omega}p_c\mathbf{v}\cdot\boldsymbol{\eta}, \tag{16}$$

where $(Z_1^{n+1}, Z_2^{n+1})\equiv\mathbf{Z}^{n+1}\in\mathscr{V}$, $\mathbf{Z}^{n+1}\approx\mathbf{z}^{n+1}$, and $S^{n+1}\in\mathscr{W}$, $S^{n+1}\approx s^{n+1}$.

Next let $\boldsymbol{\Psi}^{n+1}\in\mathscr{V}$ be an approximation to $h(s^{n+1})\mathbf{z}^{n+1}$. In particular, for $(\psi_1^{n+1}, \psi_2^{n+1})\equiv\boldsymbol{\Psi}^{n+1}$, we define

$$(\psi_1)^{n+1}_{i+1/2, j}=h^{n+1}_{i+1/2, j}(Z_1)^{n+1}_{i+1/2, j}, \tag{17}$$

where $h^{n+1}_{i+1/2, j}\equiv h((S^{n+1}_{ij}+S^{n+1}_{i+1, j})/2)$. We define $(\psi_2)^{n+1}_{i, j+1/2}$ similarly. Then, applying backward differencing in time in (5), multiplying by $w\in\mathscr{W}$ and integrating, we have that

$$\int_\Omega\frac{S^{n+1}-\bar{S}^{n+1}}{\Delta t_D}w\,dx dy+\int_\Omega\nabla\cdot\boldsymbol{\Psi}^{n+1}w\,dx dy=0. \tag{18}$$

Thus our numerical method for solving (5) is given by (16) and (18).

Setting the second component of $\mathbf{v}$ to zero in (16), applying the trapezoidal rule of integration in x and the midpoint rule in y to the integral of the first component of $\mathbf{Z}^{n+1}$, and applying the

midpoint rule to the integral involving p_c, we find that

$$(Z_1)^{n+1}_{i+1/2,j} = -\frac{(p_c)^{n+1}_{i+1,j} - (p_c)^{n+1}_{ij}}{(K^{-1})_{i+1/2,j}\Delta x}. \tag{19}$$

Applying the reverse integration rules to the integral of the second component of $\mathbf{Z}^{n+1}$ in (16), we obtain a similar expression for $(Z_2)^{n+1}_{i,j+1/2}$. Combining (18), (17) and (19), we obtain

$$\frac{S^{n+1}_{ij} - \bar{S}^{n+1}_{ij}}{\Delta t} = \frac{1}{\Delta x}\left[\frac{h^{n+1}_{i+1/2,j}}{(K^{-1})_{i+1/2,j}}\frac{(p_c)^{n+1}_{i+1,j} - (p_c)^{n+1}_{ij}}{\Delta x} - \frac{h^{n+1}_{i-1/2,j}}{(K^{-1})_{i-1/2,j}}\frac{(p_c)^{n+1}_{ij} - (p_c)^{n+1}_{i-1,j}}{\Delta x}\right] + \text{similar terms in } y. \tag{20}$$

We now apply Newton's method to (20).

The variation of the mixed method described above is superior to the standard mixed method in the following respect. In the standard mixed method, $\mathbf{z}$ would be defined by

$$\mathbf{z} = K(\mathbf{x})h(s)\nabla p_c(\mathbf{x}, s).$$

Thus the analogue of (16) would require multiplication by $h^{-1}(s)$, which, in many cases of interest in immiscible displacement, is very large or even undefined. By defining $\mathbf{z}$ as in (15), we avoid this difficulty and still allow for the use of harmonic averaging of the permeability in (19). Harmonic averaging, which involves averaging K^{-1} rather than K, has become the standard technique for handling discontinuities in permeability from one grid block to the next.

3. APPLICATIONS

The scheme described above has been applied to the simulation of gas–oil centrifuge experiments. In these experiments a core sample saturated with oil and connate water is placed in a container of gas, which is connected to a motor. The motor rotates the container, causing gas to invade the core sample and force out oil. One purpose of these experiments is to calculate relative permeability and capillary pressure curves (see e.g. References 10 and 11). Once these functions are defined, numerical simulation can be used to predict flow behaviour in the core sample. This problem is a good test for a numerical scheme. Porosity and permeability variations, capillary pressure effects, gravitational (centrifugal) effects, relative permeability and connate water must all be considered.

The particular scenarios we want to study are based on an actual laboratory experiment. The data were provided by J. Killough. In this experiment the core was 6·41 cm long and connected to a motor by an arm 13 cm in length. The relative permeability of oil, as determined from the laboratory data, was found to be

$$k_{ro} = [(0{\cdot}756 - s_g)/0{\cdot}756]^{4{\cdot}612578}, \tag{21}$$

and the measured capillary pressure curve was found to satisfy, in psi,

$$p_c^{\text{meas}} = 0{\cdot}27701\,[s_g/(1 - s_{cw} - s_g)]^{1{\cdot}70407} + 0{\cdot}34639, \tag{22}$$

where s_g is the saturation of gas. The relative permeability of gas was assumed to satisfy

$$k_{rg} = s_g^2. \tag{23}$$

The rest of the core parameters, as determined from the experiment, are given in Table I.

In the numerical simulations we made the following assumptions. At the inflow boundary, pressure was assumed to be atmospheric and gas saturation was assumed equal to $1 - s_{cw}$. At the

Table I

μ_{oil}	μ_{gas}	ρ_{oil}	ρ_{gas}	ϕ	s_{cw}	ω	K
26·36 cP	0·0114 cP	0·844 g cm^{-3}	0·00129 g cm^{-3}	0·2274	19·17%	3500 rpm	144 mD

outflow boundary, $p = p_{atm} + 6{\cdot}41 g \rho_{gas}$ and no flow of gas was assumed; no flow boundaries for pressure and saturation were assumed on the sides of the core. The gravitational force $g = \omega^2 r / g_c$, where ω is the number of rotations per minute, r is the distance from the centre of the apparatus and g_c is a gravitational constant. In these runs we assumed ω increased linearly in time from start-up and reached its maximum after 1·5 min.

In Figure 1 we compare the average oil saturation curve generated by our numerical scheme with the solution obtained in the laboratory. In the text below, this numerical solution will be referred to as the case 1 solution. As indicated in the figure, good agreement between the numerical and laboratory solutions is seen. This result serves as a validation of our numerical scheme, as well as validating the measured characteristics of the core sample. In our simulation we

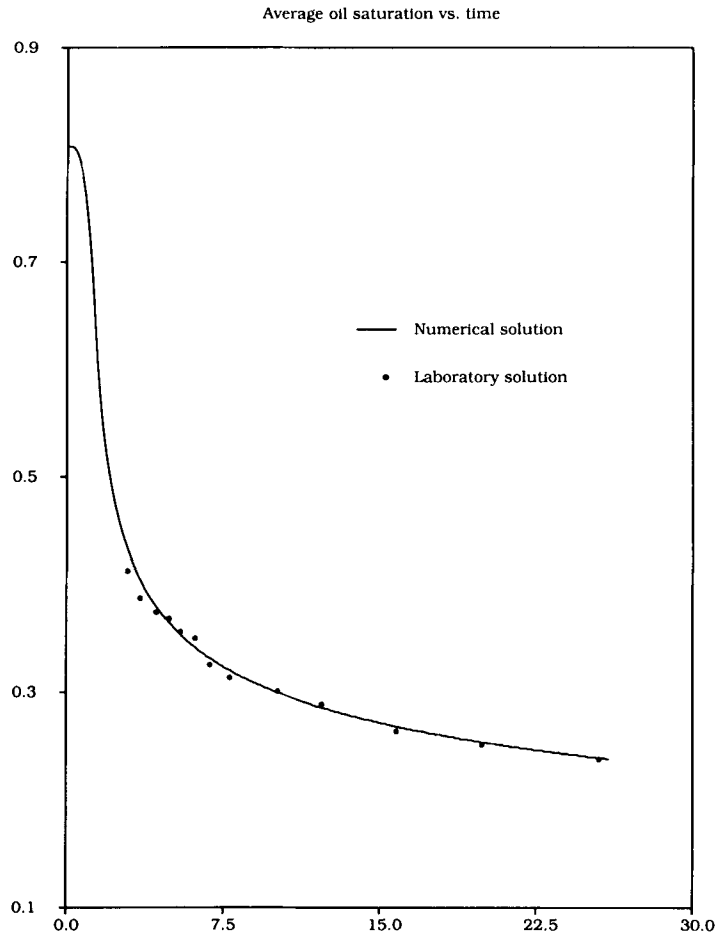

Figure 1. Numerical versus laboratory solution

used 40 grid blocks in the x-direction and three in the y-direction, and 1500 diffusion time steps were taken to simulate 28·78 min of the experiment. Our time-stepping strategy was extremely conservative. We took small time steps for advection and diffusion early in the simulation, and allowed the diffusion time step to grow slowly as the simulation proceeded.

The core sample in the laboratory experiment described above had fairly homogeneous characteristics. Hence the experiment was essentially a one-dimensional flood. This may not be the case in general. Still, there is some debate about whether two-dimensional effects are important in centrifuge simulations. In the runs described below we attempted to address this issue.

We first varied the permeability (K), leaving all other core characteristics unchanged. Two permeability fields were generated by a code written by D. Moissis.[12] This code assumes a statistical distribution of the permeabilities and allows for variations in correlation length and standard deviation. In case 2 the permeability field varied between 119 and 167 mD, and in case 3 between 57 and 290 mD. In both cases the mean permeability was 144 mD, as in the original data. In neither case did we see significant differences in the average oil saturation curves as compared to the homogeneous solution; in Figure 2 we compare the case 1 solution with the solution

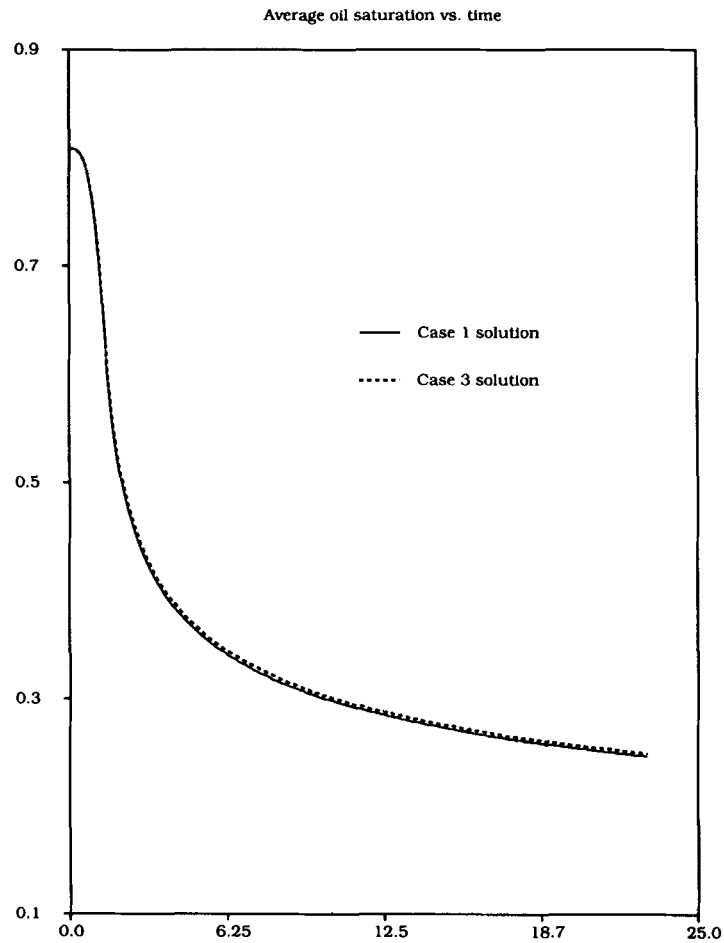

Figure 2. Case 1 versus case 3

obtained in case 3. This result is not surprising; it is commonly believed that centrifugal effects tend to override permeability effects.

Next we study the effects on the solution of both porosity and permeability variations. We considered an imaginary core sample with streaks of higher-porosity, lower-permeability rock interspersed with rock of lower porosity and higher permeability; see Figure 3. This situation is an idealization of a core with layers of chert or shale interspersed with layers of sandstone. We ran two cases, making the following assumptions. In case 4 we assumed the porosity in the shale layers was 0·4 and the permeability was 0·01 mD. In the sandstone layers the porosity was 0·17 and the permeability was 192 mD. In case 5 we assumed the porosity in the shale layers was 0·6 and the permeability was 0·001 mD, while in the sandstone layers the porosity was 0·1032, and the permeability was 192 mD. Note that in both of these cases the integral average of the porosity was 0·2274 and of the permeability 144 mD, as in case 1. In Figure 4 we compare the case 1 solution with the solutions of cases 4 and 5, and see that, as we vary the porosity and the permeability, different average oil saturation curves are obtained. In particular, oil is more reluctant to leave the core under the assumptions of cases 4 and 5 than of case 1. Moreover, the case 5 solution shows slower oil flow out of the core than the case 4 solution. These results agrees with intuition, but they also show that certain two-dimensional phenomena may be important.

In the case 4 and 5 simulations we assumed that the capillary pressure varied as a function of space and saturation. In particular, we assumed that the Leverett j-functions for the various core samples were equal, and determined a capillary pressure curve from this relationship. This assumption, suggested to us by J. Killough, is supported by heuristic evidence, which indicates that while measured capillary pressure curves may vary from core to core, the Leverett j-function remains relatively constant.[13] The Leverett j-function is given by

$$j = \alpha p_c \sqrt{\left(\frac{K}{\phi}\right)}, \tag{24}$$

where α is a proportionality constant. Thus we determined the capillary pressure for each core by the equation

$$p_c(\mathbf{x}, s) = p_c^{\text{meas}}(s) \sqrt{\left(\frac{K^{\text{meas}}}{\phi^{\text{meas}}}\right)} \sqrt{\left(\frac{\phi(\mathbf{x})}{K(\mathbf{x})}\right)}, \tag{25}$$

where p_c^{meas} is given by (22) and K^{meas} and ϕ^{meas} are the constants K and ϕ given in Table I.

In cases 4 and 5 we also assumed s_{cw} was constant throughout the core. Since this assumption is probably not realistic, we ran two cases based on the data in case 4, varying the connate water saturation as a function of space. First, in case 6, we assumed no connate water existed in the

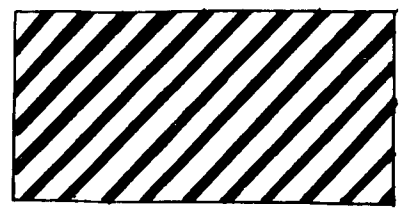

Figure 3. Permeability and porosity variations

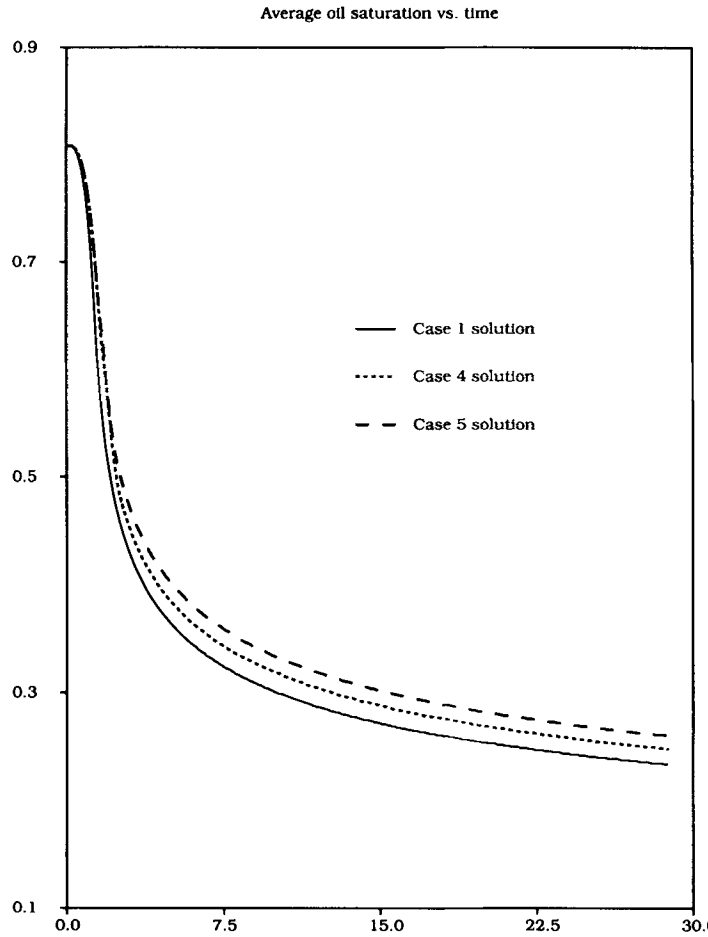

Figure 4. Case 1 versus case 4 versus case 5

sandstone layers and $s_{cw} = 0{\cdot}435$ in the shale layers. Thus the average connate water saturation over the core was still 0·1917. We allowed p_c to vary with permeability, porosity and connate water saturation through the relationships given in (22) and (25). As we can see in Figure 5, little if any effect was seen on the solution, as compared to the case 4 solution. Next we reversed the situation, allowing all the connate water to be in the sandstone layers. Again, little difference is observed from the case 4 solution; see Figure 6.

In cases 4–7 a 40×19 grid was employed, and in Figure 3 we used for comparison a case 1 solution generated on a 40×20 grid, which agrees with the case 1 solution on the 40×3 grid.

Remark 1

In our simulations we did not allow the relative permeability to vary explicitly as a function of space, which may be physically unrealistic. If future numerical testing indicates that this is an important assumption, it will be addressed in a separate paper.

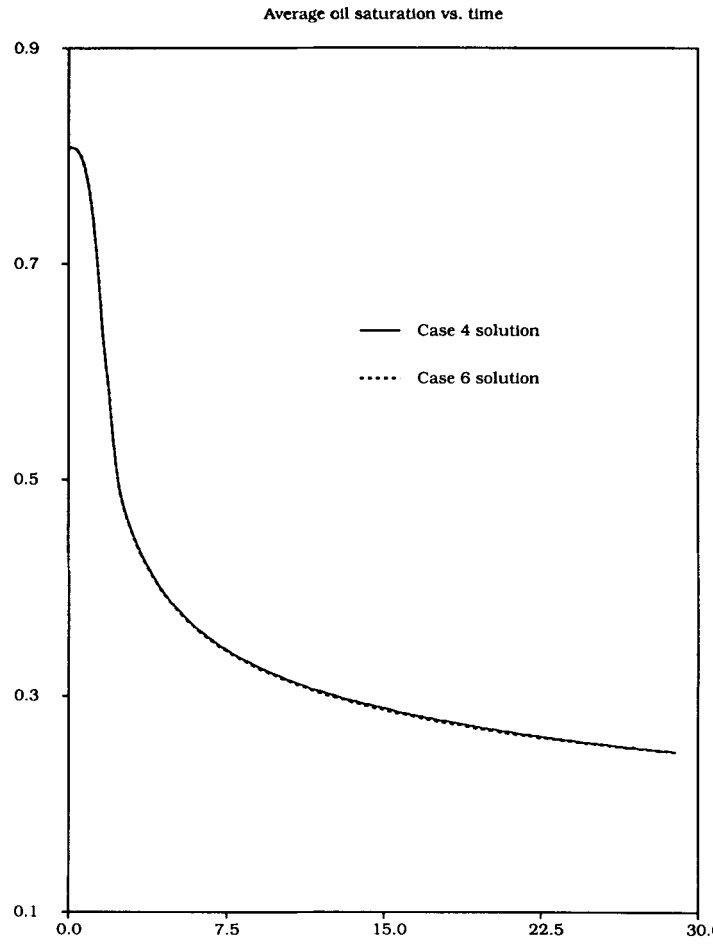

Figure 5. Case 4 versus case 6

Remark 2

The computer runs described above were performed on CRAY X-MP computers. The majority of the code is vectorized, and for the finer grid simulations took 0·2–0·3 s per time step, with the majority of the time spent in solving the non-linear system of equations given by (20). Our future research will include developing methods for improving efficiency in this piece of the calculation. We will be particularly interested in domain decomposition methods for solving (5).

4. CONCLUSIONS

In conclusion, we have developed a vectorized, two-dimensional code for modelling two-phase flow with gravity and capillary pressure. Results from centrifuge studies indicate that the code is accurate and can be used to validate laboratory models. These and earlier numerical tests indicate that the method successfully overcomes many of the numerical difficulties which plague standard simulators.

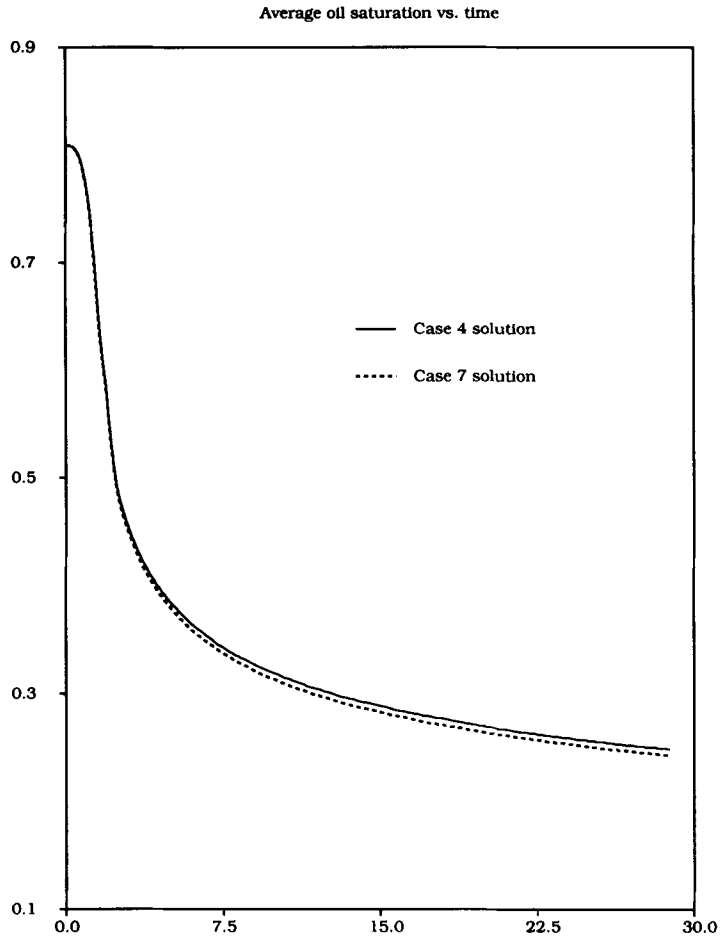

Figure 6. Case 4 versus case 7

ACKNOWLEDGEMENTS

The author would like to acknowledge the contributions of J. E. Killough, J. B. Bell, M. F. Wheeler and R. J. Blackwell to this research, and thank P. Keenan for considerable help in generating the figures.

This work was supported by NSF Grant No. DMS-8807257 and utilized the CRAY X-MP/48 computer at the National Center for Supercomputing Applications at the University of Illinois at Urbana-Champaign and the CRAY X-MP/12 computer at Argonne National Laboratory.

REFERENCES

1. G. Chavent and J. Jaffre, *Mathematical Models and Finite Elements for Reservoir Simulation*, Elsevier, New York, 1986.
2. D. Peaceman, *Fundamentals of Numerical Reservoir Simulation*, Elsevier, Amsterdam, 1977.

3. M. R. Todd, P. M. O'Dell and G. J. Hirasaki, 'Methods for increased accuracy in numerical reservoir simulators', *Soc. Petrol. Eng. J.*, **12,** 515–530 (1972).
4. G. R. Shubin and J. B. Bell, 'An analysis of the grid orientation effect in numerical simulation of miscible displacement', *Comput. Methods Appl. Mech. Eng.*, **47,** 47–71 (1983).
5. J. B. Bell, C. N. Dawson and G. R. Shubin, 'An unsplit higher order Godonov scheme for scalar conservation laws in two dimensions', *J. Comput. Phys.*, **74,** 1–24 (1988).
6. M. F. Wheeler, W. A. Kinton and C. N. Dawson, 'Time-splitting for advection-dominated parabolic problems in one space variable', *Commun. Appl. Numer. Methods*, **4,** 413–423 (1988).
7. C. N. Dawson, 'Error estimates for Godunov mixed methods for nonlinear parabolic equations', *Ph.D. Thesis*, Rice University, 1988.
8. M. F. Wheeler, 'A mixed finite element method for nonlinear diffusion problems arising in multiphase flow', in preparation.
9. P. A. Raviart and J. M. Thomas, 'A mixed finite element method for 2nd order elliptic problems', in *Mathematical Aspects of the Finite Element Method*, Rome, 1975; *Lecture Notes in Mathematics*, Springer, Berlin, 1977.
10. D. J. O'Meara Jr. and W. O. Lease, 'Multiphase relative permeability measurements using an automated centrifuge', *Paper SPE 12128, Proc. 58th Ann. Technical Conf. and Exhibition of the Society of Petroleum Engineers*, San Francisco, 1983.
11. M. J. King, A. J. Falzone, W. R. Cook, J. W. Jennings Jr. and W. H. Mills, 'Simultaneous determination of residual saturation and capillary pressure curves utilizing the ultracentrifuge', *Paper SPE 15595, Proc. 61st Ann. Technical Conf. and Exhibition of the Society of Petroleum Engineers*, New Orleans, 1986.
12. D. Moissis, 'Simulation of viscous fingering during miscible displacement in nonuniform porous media', *Ph.D. Thesis*, Rice University, 1988.
13. R. E. Collins, *Flow of Fluids through Porous Materials*, Reinhold, New York,, 1961.